Acoustic bandgaps in polyatomic chains of 3D-printed resonators

Cite as: AIP Advances 11, 125306 (2021); doi: 10.1063/5.0071874
Submitted: 18 October 2021 • Accepted: 9 November 2021 •
Published Online: 3 December 2021

Roger Domingo-Roca,[1] Euan Foster,[2] and Joseph C. Jackson-Camargo[2,a)]

AFFILIATIONS

[1] Department of Biomedical Engineering, Wolfson Building, University of Strathclyde, 106 Rottenrow East, Glasgow G4 0NW, United Kingdom
[2] Department of Electrical and Electronic Engineering, Royal College Building, University of Strathclyde, 204 George Street, Glasgow G1 1XW, United Kingdom

[a)] **Author to whom correspondence should be addressed:** joseph.jackson@strath.ac.uk

ABSTRACT

Acoustic bandgaps are ranges of frequencies in a medium at which sound cannot propagate. The classical model often used in solid-state physics is that of a 1D chain of masses and springs, the analysis of which can predict the speed of sound in a material, its dispersive nature, and any forbidden sound frequencies. We use a lumped parameter model for the acoustic inertance and compliance of pipes and cavities to create 1D monatomic, diatomic, and triatomic chains that demonstrate these acoustic bandgaps experimentally. The ease of 3D-printing these devices means that this method can be used to explore bandgap engineering in acoustic systems for low-frequency applications and used as a simple platform for creating acoustic analogs of the solid-state physical problem. Furthermore, it allows us to explore novel polyatomic behavior (e.g., tetratomic and pentatomic) and could ultimately find use as filters for experiments requiring miniaturized acoustic isolation.

I. INTRODUCTION

An acoustic bandgap in a material is defined as a band of frequencies at which a sound wave cannot propagate—instead, the wavenumber of the wave solution is imaginary—and rather than propagating, acoustic excitations decay. Bandgaps can be created in bespoke materials to create the so-called acoustic metamaterials[1,2] that constitute an exciting area of research in which the material structure, rather than material properties, shapes the behavior of sound propagation.[3] Real world applications of this research span all acoustic domains, from seismology studies, building acoustics, underwater acoustics, and high-frequency ultrasonics.[4–6] Shielding a building from an earthquake, improving SONAR for underwater vehicle navigation, cloaking objects from airborne sound,[7] and controlling vibration noise in building materials are just some of the myriad applications.[1,2] One potential use of acoustic metamaterials is to provide deep attenuation of sound by engineering bandgaps at certain frequencies where sound cannot propagate.[4]

Acoustic metamaterials, and the meta-atoms from which they are built, are not easy to make. For a given frequency range, the contrasting scale between the material and meta-atom means that manufacturing is difficult and sometimes impossible (or at least certainly not economical) despite what may be possible from a theoretical perspective. The goal for many applications is to make a mesoscale structure with microscale features, and the promising technology is 3D printing, a form of additive manufacturing that is fast becoming ubiquitous in scientific research due to its speed, scale, and now decreasing cost. 3D printing has been a key tool in the development of practical acoustic resonators and acoustic metamaterials.[8,9]

It is clear that the development of practical acoustic metamaterials is a fine balance between structural (and perhaps the material) complexity that enriches the acoustic behavior of a system and feasibility of manufacturing, which is perhaps why despite decades of research into the acoustics of structured materials, one will struggle to encounter an acoustic metamaterial in the real world (although nature can often be counted on to do something that engineers and physicists cannot[10]). For that reason, we were motivated to explore simple acoustic arrangements that can be 3D-printed at small and large scales, which can lead to acoustic bandgaps, the central physics behind metamaterial research.[4] We took inspiration from the solid-state physics that is often used pedagogically to introduce the concepts of bandgaps in acoustics.[1,2]

A simple model used to illustrate the generations of bandgaps is a 1D chain of masses and springs [Fig. 1(a)]. Common in solid-state

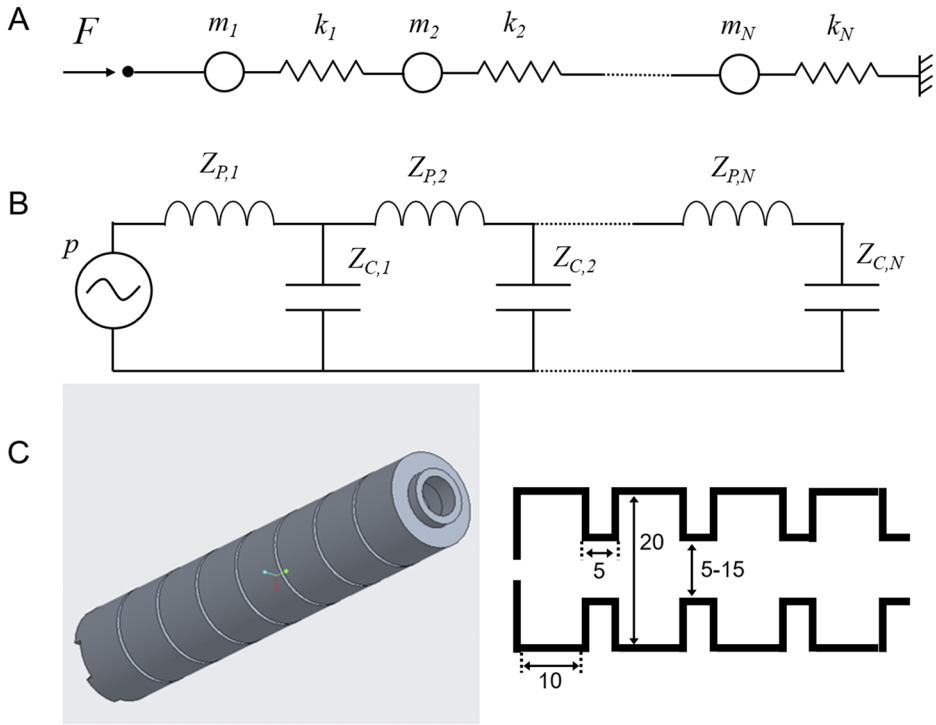

FIG. 1. (a) A chain of masses and springs used as models for many physical phenomena. (b) Lumped parameter model of acoustic inertances and acoustic compliances analogous to the 1D chain of the mass-spring model. (c) (Left) CAD model for 3D-printing of an acoustic oscillator chain, in this case monatomic, with each pipe and cavity being identical. (Right) Schematic of 3D-printed part (dimensions in mm), where all geometry is fixed for the pipe radius, which could be 5 mm throughout, alternating 5 and 7.5 mm, or alternating 2.5, 5, and 7.5 mm for the monatomic, diatomic, and triatomic chains, respectively. Note the port at the (left) end of the chain, into which a microphone can be inserted.

physics,[11] this model can be solved to reveal the dispersion characteristics of a putative solid (i.e., the relationship between the angular frequency ω and the wavenumber k) and thus both the speed of sound in the material and any forbidden frequencies where sound does not propagate but is instead evanescent. The simplest model is the monatomic chain where masses m and springs (with Hookean stiffness k_H) are all equal and spaced evenly. It is well known that in this model, for long wavelengths, the speed of sound is constant and non-dispersive, and as the wavelength decreases toward the scale of an individual mass-spring system, the speed of sound (or $\partial\omega/\partial k$) decreases to zero. These models are easily solved[11] using an ansatz that solutions are of the form $u(t,x) = Ae^{i(k+i\delta)x-i\omega t}$, from which both the propagating wavenumber k and an evanescent decay wavenumber δ can be derived to create dispersion curves. These graphs can be found in most solid-state physics textbooks.

In the monatomic chain, above a certain cut-off frequency $\omega = (2\sqrt{k_H/m})$, no sound propagation is possible. As we approach this cut-off frequency, the speed of sound in the chain decreases, becoming zero at the edge of the Brillouin zone.[11] Beyond this frequency, evanescent solutions exist for a penetration-wavenumber δ inversely proportional to the penetration depth of the sound into the chain. The depth of this penetration decreases as the frequency increases. The next simplest model is the diatomic chain, in which successive masses are not equal, and the repeating unit is two masses m_1 and m_2 connected via springs of stiffness k_H. In this model, the dispersion curve is split into two curves (the so-called acoustic and optical branches) separated by a forbidden band, providing $m_1 \neq m_2$. The upper frequency limit, above which no sound can propagate, is at $\omega = \sqrt{2k_H/\mu}$, where μ is the reduced mass $\frac{m_1 m_2}{m_1+m_2}$.

One can increase the complexity of the model system introducing more masses (e.g., triatomic chains with three bandgaps) or changing the stiffness of the bonds between masses, but each additional complexity makes the analysis more difficult. Mathematical studies on *polyatomic* chains have been performed to reveal the rich dynamics of such systems.[12]

Our objective is to explore acoustic analogs of these systems that have dispersive features at practical relevant audible frequencies rather than the terahertz frequencies found in solid-state physics models. We do this for a variety of reasons—pedagogical and investigative. Specifically, these polyatomic systems act as almost ideal low-pass filters, and the diatomic and triatomic models have additional band-stop filters between the acoustic and optical branches. To that end, we utilize the mechanical–acoustic analogy, replacing masses with acoustic inertances and springs with acoustic compliances, and we consider them lumped parameters as we intend to create systems much smaller than the wavelength of sound with which they interact.

In the low-frequency limit, where the size of an acoustic system is much smaller than the wavelength of sound with which it interacts, an acoustic inertance can be modeled as a pipe with a normalized acoustic impedance $Z_P = i\omega$, in which air moves as a mass and any air compression is negligible. In contrast, an acoustic compliance can be modeled as a cavity with a normalized acoustic impedance $Z_C = -i/\omega$, in which the acoustic volume flow is dominated by compression. Thus, a 1D chain of masses and springs can be replaced with a chain of pipes and cavities. Given that a pipe-cavity system is the classic Helmholtz resonator, the 1D chain could alternatively be described as a chain of Helmholtz resonators connected serially. Note that on applying the low-frequency limit, we

lose the dependence of the impedance on the wavenumber k, and thus, we no longer think of spatial extent of the pipes and cavities as relevant to the bandgap generation, provided that we always adhere to the limit of low frequency. From an engineering perspective, if one wishes to create devices operating at audio frequencies that are, for example, wearable, then the restriction that an acoustic component be smaller than the wavelength of the sound it interacts with is satisfied by default.

We can modify the inertance and compliance (and therefore the mass and spring equivalent values) simply by modifying the geometry of the pipes and cavities in the chain. Hence, with 3D-printing technology, we can explore polyatomic chains (for example, by varying the pipe dimensions) and in addition explore chains with differing spring stiffnesses (i.e., by varying the cavity dimensions). In the rest of this paper, we limit ourselves to the monatomic, diatomic, and triatomic systems, and we first discuss finite chains, their eigenfrequencies, and how they approximate the infinite chain. We conclude with an experimental demonstration of three devices that reproduce the bandgap properties of modeled systems with practical audible acoustic frequencies.

II. FINITE CHAINS OF PIPES AND CAVITIES

A finite chain of pipes and cavities is represented by the acoustic circuit shown in Fig. 1(b), relating the acoustic pressure p to the acoustic volume flow U and the total acoustic impedance Z_N through $p = UZ_N$. We can solve this by computing the total impedance of the system and finding solutions for when the imaginary part of the impedance is zero. Of course, there are other methods available, such as the reflection/transmission method in Ref. 13 or the matrix method for the equations of motion as used in Ref. 14. The total impedance Z_N of a chain of N Helmholtz resonators can be calculated using the acoustic impedance of the n^{th} Helmholtz resonator, i.e., the pipe $Z_{P,n}$ and cavity $Z_{C,n}$. The first three equations are as follows:

$$\begin{aligned} Z_1 &= Z_{P,1} + Z_{C,1}, \\ Z_2 &= Z_{P,1} + Z_{C,1} \| (Z_{P,2} + Z_{C,2}), \\ Z_3 &= Z_{P,1} + Z_{C,1} \| (Z_{P,2} + Z_{C,2} \| (Z_{P,3} + Z_{C,3})), \end{aligned} \tag{1}$$

where $\|$ is a parallel operator defined as $a \| b = \frac{ab}{a+b}$. To calculate the acoustic impedance of a chain of N Helmholtz resonators Z_N, we can take the impedance Z_{N-1} and replace the last cavity impedance with the parallel combination of said cavity impedance and next (and last) Helmholtz resonator. Resonance can be found by solving $Z_N = 0$, which, in the absence of a real (dissipative) part in the impedances, leads to infinite acoustic volume flow for finite pressure input. Solving $Z_N = 0$ leads to polynomials in ω^2 of order N. Including dissipation in the pipe or cavity impedances results in the acoustic impedance not approaching zero at the eigenfrequencies but instead of being a local minimum. Dissipation is difficult to quantify in general, so experimental approaches are needed to determine the strength of both the resonances and the expected attenuation of a real acoustic system.

A. Finite monatomic chains of pipes and cavities

For a monatomic chain, we consider that the unit cell of the chain is one Helmholtz resonator of fixed geometry such that the generating functions are as follows:

$$\begin{aligned} Z_1 &= Z_P + Z_C, \\ Z_2 &= Z_P + Z_C \| (Z_P + Z_C), \\ Z_3 &= Z_P + Z_C \| (Z_P + Z_C \| (Z_P + Z_C)), \end{aligned} \tag{2}$$

where we limit ourselves to the first three equations, i.e., chains of one, two, and three Helmholtz resonators. In the low-frequency limit, the impedances in Eq. (2) can be replaced by their normalized Fourier equivalents $Z_P = i\omega$ and $Z_C = -i/\omega$ and solved to compute the eigenfrequencies ω_N. The first case, $Z_1 = 0$, leads to the solution for the normalized resonant frequency of the Helmholtz frequency, $\omega_1 = 1$. The first three equations, and their corresponding positive real solutions, are as follows:

$$\begin{aligned} \omega_1^2 - 1 = 0 &\Rightarrow \omega_1 = 1, \\ \omega_2^4 - 3\omega_2^2 + 1 = 0 &\Rightarrow \omega_2 = \frac{1}{2}\left(\sqrt{5} \pm 1\right) \approx 0.62, 1.62, \\ \omega_3^6 - 5\omega_3^4 + 6\omega_3^2 - 1 = 0 &\Rightarrow \omega_3 \approx 0.45, 1.25, 1.80. \end{aligned}$$

A chain of N Helmholtz resonators has N positive unique eigenfrequencies, the maximum of which tends toward the infinite chain cut-off frequency $2\omega_1$. As $N \to \infty$, the eigenfrequencies become a continuum of eigenstates bounded from 0 to $2\omega_1$. Figure 2(a) shows the evolution of eigenvalues with increasing N. If we wish to visualize the acoustic spectral response, we can do so by plotting $|Z_N^{-1}|$, which is the acoustic volume flow into the chain; it consists of N peaks corresponding to resonances, followed by a zone of no propagating solutions. Clearly, this system is an acoustic low-pass filter in the low-frequency limit.

B. Finite diatomic chains of pipes and cavities

The acoustic circuit of a finite diatomic chain again follows the schema in Fig. 1(b). We define the pipe impedance as $Z_{P,n}$ for the n odd and $\alpha Z_{P,n}$ when n is even. The parameter α scales the geometry of the neck. The definition can be used similar to Eq. (1) to calculate the eigenfrequencies of a diatomic system,

$$\begin{aligned} Z_1 &= Z_P + Z_C, \\ Z_2 &= Z_P + Z_C \| (\alpha Z_P + Z_C), \\ Z_3 &= Z_P + Z_C \| (\alpha Z_P + Z_C \| (Z_P + Z_C)). \end{aligned} \tag{3}$$

The evolution of the eigenfrequencies can be seen in Fig. 2(b) where the increasing number of Helmholtz resonators reveals the acoustic behavior of the system. In this definition, there are N positive eigenfrequencies, and in the limit of $N \to \infty$, the eigenvalues form a continuum and the maximum value approaches the cut-off frequency for the infinite diatomic chain. However, in agreement with the solid-state representation of diatomic chains, there exists a bandgap between the N solutions. It is well known from solid-state theory that the bandgap width is controlled by the masses and springs of the chain,[11] and the same is true here; we can control the bandgap and the upper cut-off frequency by choosing the geometry of the pipe and cavity carefully, which essentially governs the acoustic inertance and compliance, respectively. As we shall see

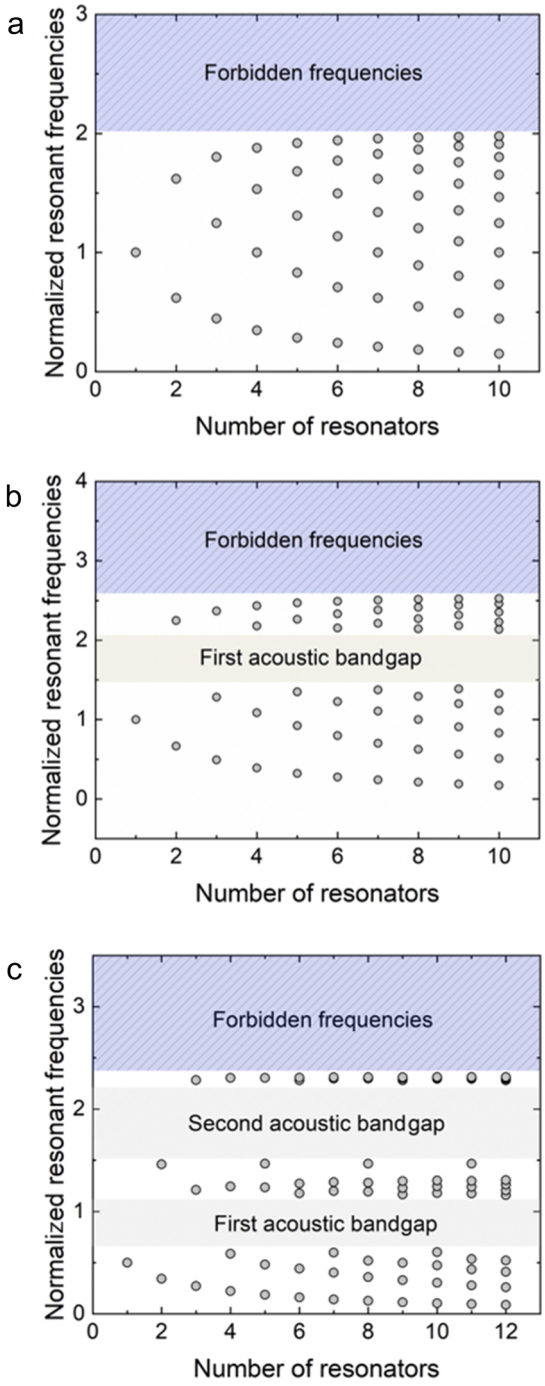

FIG. 2. Eigenvalues of finite chains of Helmholtz resonators, normalized such that the first individual resonator has unity resonance frequency. For all systems, there is an upper cut-off frequency above which no propagating solutions exist—at least within the restriction that the individual resonator is much smaller than the acoustic wavelength. (a) Monatomic eigenfrequencies. A family of N positive real eigenfrequencies exist. (b) Diatomic eigenfrequencies with $\alpha = 1.5^{-2}$. A bandgap appears between the eigenstates in addition to the upper cut-off range. (c) Triatomic eigenfrequencies with $\alpha = 1.5^{-2}$ and $\beta = 0.5^{-2}$. There are two acoustic bandgaps and an upper cut-off.

later, choosing $\alpha = 1.5^{-2}$ is convenient in that it corresponds approximately to an increase in the pipe radius of 50%. Given that value, the first few solutions are as follows:

$$\omega_1 = 1,$$
$$\omega_2 = \sqrt{\frac{2+\alpha+\sqrt{\alpha^2+4}}{2\alpha}} \approx 0.67, 2.25,$$
$$\omega_3 \approx 0.49, 1.28, 2.37.$$

Of course, the first eigenmode in Fig. 2(b) is only included for completeness, as the chain of only one Helmholtz resonator cannot in any meaningful way said to be diatomic.

C. Finite triatomic chains of pipes and cavities

For a triatomic chain, we start with the pipe impedance of the first Helmholtz resonator with an impedance βZ_P and state that for the three-resonator unit cell, the second pipe has an impedance Z_P and the third pipe has an impedance αZ_P. For clarity and brevity, we only reproduce as an example the Z_3 equations as follows:

$$Z_3 = \beta Z_P + Z_C \| (Z_P + Z_C \| (\alpha Z_P + Z_C)). \tag{4}$$

Again, we use Eq. (1), nesting the introduction of a new impedance modeling a Helmholtz resonator, to deduce the positive eigenfrequencies using the normalized Fourier impedances $Z_P = i\omega$ and $Z_C = -i/\omega$. The solutions as a function of total number of resonators N are shown in Fig. 2(c) where we have chosen $\alpha = 1.5^{-2}$ and $\beta = 0.5^{-2}$, which could practically be said to correspond to an increase or decrease in the pipe radius [see Eqs. (5) and (6)]. We see, as expected, two bandgaps in the limit of $N \to \infty$ and an upper cut-off frequency. Note that, similar to the diatomic case, the first two eigenmodes in Fig. 2(c) are only included for completeness—we require at least three Helmholtz resonators to form a triatomic chain.

While in this paper we have chosen to restrict ourselves to the three cases (monatomic, diatomic, and triatomic), there is no reason why one could not investigate tetratomic, pentatomic, or any of the Greek cardinal prefixes, knowing that increasing the number of distinct *masses* or inertances in the chain will increase the number of bandgaps and that we can also change the compliance through the cavity dimensions. There is therefore large scope to explore models beyond the confines of solid-state physics, should there be an advantage in doing so.

D. Experimental methods

Three chains of Helmholtz resonators were designed to explore bandgaps in polyatomic chains. We chose to focus on monatomic, diatomic, and triatomic chains although there is little barrier to expanding to any number of different Helmholtz resonators that, when combined, form the unit cell. Each chain comprises a series connection of pipes and cavities formed as cylinders, with dimensions as follows: cavity radius, 10 mm; cavity length, 10 mm; and pipe length, 5 mm (Fig. 3). The pipe radius was a parameter to be modified in design to create changes in the resonator inertance along the chain. For the monatomic case, the pipe radius was 5 mm; for the diatomic case, pipe radii were 5 and 7.5 mm sequentially; and for the triatomic case, pipe radii were 5, 7.5, and 2.5 mm. These choices

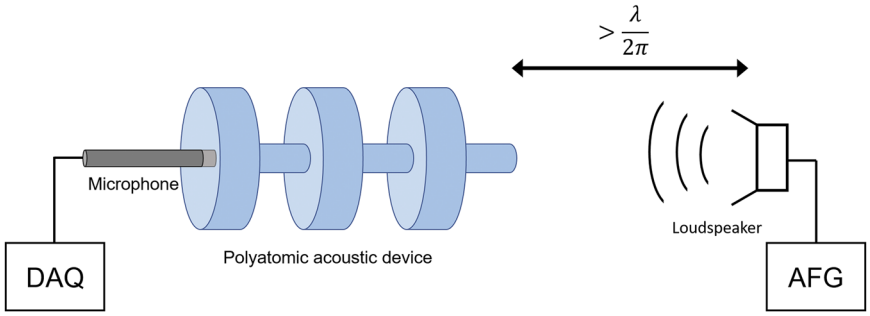

FIG. 3. Experimental setup. The printed device is a chain of pipes and cavities. The aperture for sound to enter is a pipe, and there is a 4 mm hole in the terminating cavity into which a microphone is placed. Sound is played from a loudspeaker at a distance $>\lambda/2\pi$ from the device to ensure that the sound is in the far field. An arbitrary function generator (AFG) provides the loudspeaker signal, and microphone data are recorded with a data acquisition (DAQ). The polyatomic acoustic device geometry is exaggerated for ease of viewing.

ensured that the real 3D-printed acoustic devices matched the relative changes in pipe impedance used in Fig. 2. Note that the pipe radii chosen for the diatomic and triatomic chains correspond to scaling factors $\alpha = 1.5^{-2}$ and $\beta = 0.5^{-2}$. A real Helmholtz resonator has pipe and cavity impedances as follows:

$$Z_P = \frac{i\rho\omega L}{S}, \qquad Z_C = \frac{-i\rho c^2}{\omega V}, \tag{5}$$

respectively, and therefore, it has a resonant frequency $f = \omega/2\pi$ given by

$$f = \frac{c}{2\pi}\sqrt{\frac{S}{LV}}, \tag{6}$$

where c is the speed of sound in air, ρ is the density of air, S is the cross-sectional area of the pipe, L is the length of the pipe (subject to the addition of an end correction $1.2a$, where a is the pipe radius), and V is the cavity volume. The dimensions of the printed part means that for the monatomic case, a single Helmholtz resonator should have a resonant frequency of 2.6 kHz and the infinite chain should have an upper cut-off frequency of ~5.2 kHz. Bandgaps can be predicted from Fig. 2 noting that the base frequency (i.e., when $N = 1$) is 2.6 kHz.

Eight Helmholtz resonators (a pipe and a cavity in series) were 3D-printed with geometries corresponding to the monatomic and diatomic cases and nine resonators for the triatomic case. Computer-aided design files (.stl) of the chains were designed using PTC Creo Parametric, with a wall thickness of 1 mm [e.g., Fig. 1(c)]. A 4 mm hole was included in the last cavity as a port to place a 1/8 in. microphone (Bruel and Kjaer, 4138, with preamplifier 2670, Naerum, Denmark). The STL models were sliced with proprietary software for the stereolithography (SLA) 3D printer Prusa SL1 (Prague, Czech Republic), and models were printed with 100 μm layer thickness in a UV-curable polymer (Prusa Gray Tenacity, Prusa, Prague, Czech Republic). Cured devices were washed with isopropyl alcohol (Sigma-Aldrich, MO, USA) to remove the uncured polymer and subsequently cured in UV light (Prusa CL1, Prusa, Czech Republic). While the target frequency for the individual monatomic Helmholtz resonator was ~2.6 kHz, in practice, this is not guaranteed as the equations governing the low-frequency approximation have corrections due to boundary-layer losses or end corrections to pipe lengths that model the radiation transition impedance.

Figure 3 shows a schematic of the experiment. All experiments were conducted in an acoustic isolation booth. A 4 in. loudspeaker was driven from the internal generator of the acquisition system of a Laser Doppler vibrometer (MSA-100-3D, Polytec, Waldbronn, Germany) via a power amplifier (SANYO TA-FE370, Tokyo, Japan). From this source at a distance of 50 cm, the B&K 1/8 in. microphone was placed. Reference measurements were taken prior to the device measurement, against which the results were normalized. A periodic chirp from 100 Hz to 20 kHz was played at the device, and the microphone signal was amplified and conditioned (Conditioning amplifier Nexus 2690, Bruel and Kjaer, Naerum, Denmark) with an electrical output of 100 mV/Pa. Data were recorded using the data acquisition system of the vibrometer, and the sound level was manually adjusted and corrected to create a sound signal with a flat spectrum at a sound pressure level of ~60 dB SPL (re. 20μPa). Experimental data are stored at the Strathclyde KnowledgeBase repository.[15]

III. RESULTS AND DISCUSSION

The three devices have eigenmodes and bandgaps that can be calculated using the iterative method highlighted in Eqs. (2)–(4). This was performed using Mathematica (v. 12.2, Champaign, IL, USA), and the analysis involves finding the roots of a polynomial

TABLE I. Positive real eigenfrequencies.

Monatomic (kHz)	Diatomic (kHz)	Triatomic (kHz)
0.48	0.55	0.30
1.42	1.63	0.87
2.32	2.60	1.29
3.13	3.36	3.03
3.84	5.57	3.20
4.42	5.90	3.37
4.85	6.28	5.93
5.11	6.54	5.98
...	...	6.01

in ω of order $2N$, where N is the number of resonators in the chain. For the eight-element monatomic and diatomic chains and the nine-element triatomic chain, the solutions for the eigenfrequencies can be found in Fig. 2, but they are shown for the experimental devices in Table I.

The monatomic and diatomic devices show the existence of eight resonances, while the triatomic device shows nine peaks above which for all devices follows strong attenuation above the expected cut-off frequency, which can be seen in Fig. 4. The diatomic device includes the intermediate bandgap, and similarly, the triatomic device shows two intermediate bandgaps [Fig. 4(c)]. The upper bandgap, which theoretically extends to infinity, fails above around 15 kHz. Most likely, this is due to the breakdown of the model that assumes that the resonators are larger than the sound wavelength, but at 15 kHz, the wavelength is ≈2 cm, which approaches the scale of individual resonators. Further attenuation at higher frequencies may be due to overtones within the cavities, leading to Bragg interference (which underpins phononic crystals), which the lumped parameter model does not take into account. The devices show strong amplification of sound at the eigenfrequencies (~20 dB above the sound input) and strong attenuation (~30–40 dB below the sound input) in the bandgaps. For the diatomic and triatomic devices, the intermediate bandgaps show less attenuation (~20 dB), which may be due to the longer penetration depth of evanescent sound within these bands predicted by solid-state models. In this model, the intermediate bandgaps (red lines) can have small values for δ. As the solution to these models goes as $\sim e^{-\delta x}$, sound can penetrate further down the chain as $\delta \to 0$. Thus, we expect deeper attenuation of sound for the upper cut-off frequencies and for frequencies that are far away from real propagating solutions. The data in Table I do not exactly match the position of the experimental peaks and gaps in Fig. 4. There are multiple explanations for this. The most prosaic explanation is that the modeled calculated impedances are not sufficiently accurate. There will be corrections to the ideal impedances due to the shapes of the pipes and cavities. Friction reduces the apparent volumes, and radiation transition impedances lead to corrections in pipe lengths. Furthermore, the impedances of the first pipe and last cavity will be different from those of the other pipes and cavities due to the transition to free space and the microphone porthole, respectively. However, it is clear that the theoretical prediction and experimental outcome follow the same pattern.

We have shown that the chains of Helmholtz resonators can be 3D-printed and exhibit acoustic bandgaps. There is surprisingly little in the literature on chains of polyatomic units of pipes and cavities *in series* as the basis for acoustic bandgap engineering. There have been studies on 1D chains similar to our investigations, exploring defects in monatomic chains,[13] and in addition, there has been work on chains of spheres, such as diatomic chains in Refs. 14, 16. For acoustic resonators, Helmholtz resonators are used in parallel extensively,[17] either to modify the propagation of sound within a duct[17,18] or as part of a metasurface.[19] Chains of membrane-based systems in which the membranes are stacked in series have been studied,[20] but the acoustic analog of a membrane consists of both an inertance and a capacitance and as such does not match these solid-state models in spirit. One similar situation has been described in which a face-centered cubic lattice of Helmholtz resonators was printed,[21] which does indeed show rich acoustic behavior, although it is essentially a monatomic crystal.

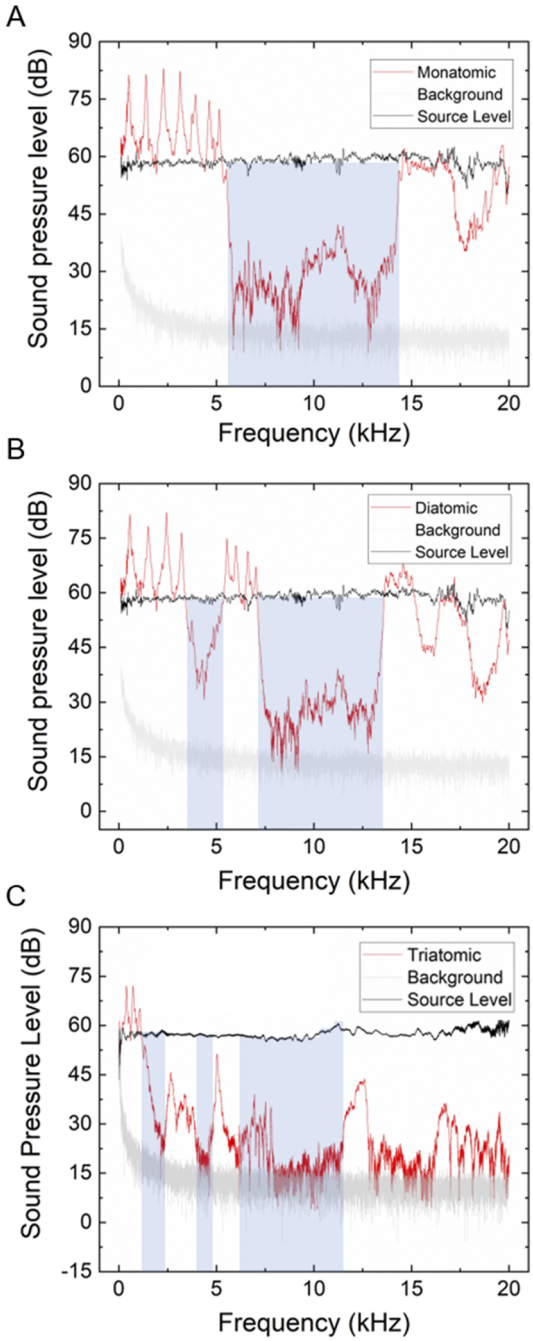

FIG. 4. Bandgaps (shaded) in monatomic, diatomic, and triatomic chains of pipes and cavities. The sound stimulus was 50 dB SPL across all frequencies. (a) Monatomic chain attenuation. Eight peaks (corresponding to eigenstates of the eight-chain device) are visible up to ~5.6 kHz, at which point the bandgap begins. After 10 kHz, the low-frequency approximation fails. (b) Diatomic chain. Two bandgaps appear at ~4 kHz and above 7 kHz, corresponding to the split between the acoustic and optical branches of the infinite model and the high-frequency cut-off, respectively. The attenuation falls to the experimental noise floor. There exists a third bandgap at 17–18 kHz, not due to the physics described here. (c) Triatomic chain. There are three bandgaps as expected. Note that they all behave as the trend expected in Fig. 2.

Chains of complex meta-atoms have been shown to have rich behavior as well,[22] but again, these are still effectively monatomic lattices.

The increasingly easy methods to produce complex geometries are opening up the manufacture of structured materials for practical low-cost bandgap engineered systems.[8] In this article, we have shown that simple chains of pipes and cavities exhibit properties that correlate, unsurprisingly, with known behaviors of solid-state models and can be used pedagogically. This work can be expanded in three ways: (1) the miniaturization of such chains or the stacking of 1D chains to create materials. Care must be taken when miniaturization occurs, as end corrections for pipe lengths and viscous losses can significantly alter the expected behavior. (2) The exploration of the acoustic properties of chains with more than three distinct resonators within the unit cell and with both different masses and different springs. (3) One could imagine simple chains being stacked and *connected* with 2D and 3D arrays of these resonators to explore acoustic analogs of wave propagation in solids and bandgap engineering. This has been demonstrated in lattice networks of Helmholtz resonators,[21] but as noted earlier, these were effectively monatomic chains. Finally, we note that the experimental results highlight the incredibly powerful amplification (outside the band) and attenuation (within the band) properties of these chains that could be used for bespoke, cheap signal conditioning of acoustic signals to improve the signal-to-noise ratio and thus the sensitivity of an acoustic experimental situation.

ACKNOWLEDGMENTS

We would like to thank staff at the Centre for Ultrasonic Engineering (University of Strathclyde), in particular Paul Daly, for useful help and discussions. This work was supported, in part, by Grant No. EP/L022125/1 (E.F.) and Grant No. EP/S023879/1 (facilities and equipment).

AUTHOR DECLARATIONS

Conflict of Interest

The authors have no conflicts to disclose.

DATA AVAILABILITY

The data that support the findings of this study are openly available in the University of Strathclyde KnowledgeBase repository at https://doi.org/10.15129/e785e5b0-0f2e-4bd6-bddd-09c7555066a8.

REFERENCES

[1] *Acoustic Metamaterials*, edited by R. Craster and S. Guenneau (Springer Netherlands, 2013), Vol. 166.
[2] *Fundamentals and Applications of Acoustic Metamaterials*, edited by A.-C. Hladky-Hennion and V. Romero-Garcia (Springer Netherlands, 2019), Vol. 1.
[3] G. Liao, C. Luan, Z. Wang, J. Liu, X. Yao, and J. Fu, "Acoustic metamaterials: A review of theories, structures, fabrication approaches, and applications," Adv. Mater. Technol. **6**, 2000787 (2021).
[4] S. Kumar and H. Lee, "The present and future role of acoustic metamaterials for architectural and urban noise mitigations," Acoustics **1**, 590–607 (2019).
[5] S. Brûlé, E. H. Javelaud, S. Enoch, and S. Guenneau, "Experiments on seismic metamaterials: Molding surface waves," Phys. Rev. Lett. **112**, 133901 (2014).
[6] Z. Li, S. Yang, D. Wang, H. Shan, D. Chen, C. Fei, M. Xiao, and Y. Yang, "Focus of ultrasonic underwater sound with 3D printed phononic crystal," Appl. Phys. Lett. **119**, 073501 (2021).
[7] C. Liu, J. Shi, W. Zhao, X. Zhou, C. Ma, R. Peng, M. Wang, Z. H. Hang, X. Liu, J. Christensen, N. X. Fang, and Y. Lai, "Three-dimensional soundproof acoustic metacage," Phys. Rev. Lett. **127**, 084301 (2021).
[8] A. Gardiner, P. Daly, R. Domingo-Roca, J. F. C. Windmill, A. Feeney, and J. C. Jackson-Camargo, "Additive manufacture of small-scale metamaterial structures for acoustic and ultrasonic applications," Micromachines **12**, 634 (2021).
[9] M. Askari, D. A. Hutchins, P. J. Thomas, L. Astolfi, R. L. Watson, M. Abdi, M. Ricci, S. Laureti, L. Nie, S. Freear, R. Wildman, C. Tuck, M. Clarke, E. Woods, and A. T. Clare, "Additive manufacturing of metamaterials: A review," Addit. Manuf. **36**, 101562 (2020).
[10] T. R. Neil, Z. Shen, D. Robert, B. W. Drinkwater, and M. W. Holderied, "Moth wings are acoustic metamaterials," Proc. Natl. Acad. Sci. U. S. A. **117**, 31134–31141 (2020).
[11] C. Kittel, *Introduction to Solid State Physics* (Wiley, 2018).
[12] H. Al Ba'na'a, M. Nouh, and T. Singh, "Dispersion and topological characteristics of permutative polyatomic phononic crystals," Proc. R. Soc. London, Ser. A **475**, 20190022 (2019).
[13] J. N. Munday, C. B. Bennett, and W. M. Robertson, "Band gaps and defect modes in periodically structured waveguides," J. Acoust. Soc. Am. **112**, 1353–1358 (2002).
[14] A.-C. Hladky-Hennion, G. Allan, and M. de Billy, "Localized modes in a one-dimensional diatomic chain of coupled spheres," J. Appl. Phys. **98**, 054909 (2005).
[15] R. Domingo-Roca, E. Foster, and J. Jackson-Camargo, Data for: 'Acoustic band gaps in polyatomic chains of 3D-printed resonators,' University of Strathclyde, 2021, https://doi.org/10.15129/e785e5b0-0f2e-4bd6-bddd-09c7555066a8.
[16] A.-C. Hladky-Hennion and M. de Billy, "Experimental validation of band gaps and localization in a one-dimensional diatomic phononic crystal," J. Acoust. Soc. Am. **122**, 2594–2600 (2007).
[17] N. Fang, D. Xi, J. Xu, M. Ambati, W. Srituravanich, C. Sun, and X. Zhang, "Ultrasonic metamaterials with negative modulus," Nat. Mater. **5**, 452–456 (2006).
[18] Z. G. Wang, S. H. Lee, C. K. Kim, C. M. Park, K. Nahm, and S. A. Nikitov, "Acoustic wave propagation in one-dimensional phononic crystals containing Helmholtz resonators," J. Appl. Phys. **103**, 064907 (2008).
[19] Y. Zhu and B. Assouar, "Multifunctional acoustic metasurface based on an array of Helmholtz resonators," Phys. Rev. B **99**, 174109 (2019).
[20] S. H. Lee, C. M. Park, Y. M. Seo, Z. G. Wang, and C. K. Kim, "Composite acoustic medium with simultaneously negative density and modulus," Phys. Rev. Lett. **104**, 054301 (2010).
[21] A. Biçer, N. Korozlu, O. A. Kaya, and A. Cicek, "Broad omnidirectional acoustic band gaps in a three-dimensional phononic crystal composed of face-centered cubic Helmholtz resonator network," J. Acoust. Soc. Am. **150**, 1591–1596 (2021).
[22] O. R. Bilal, D. Ballagi, and C. Daraio, "Architected lattices for simultaneous broadband attenuation of airborne sound and mechanical vibrations in all directions," Phys. Rev. Appl. **10**, 054060 (2018).